Vol. 92 No. 1 pp. 268–285 ACTA GEOLOGICA SINICA (English Edition) Feb. 2018

Sedimentology and Sequence Stratigraphy of Marine to Lacustrine Deltaic Deposits in a Craton Basin and Their Controlling Factors: Shan 2 Member–He 8 Member (Guadalupian–Lopingian, Permian), Southeast Ordos Basin, North China

SHAN Xin[1], YU Xinghe[2*], HAN Xiaoqin[3],CLIFT Peter [4],ZHOU Jinsong[3], DU Yonghui[3], LI Yalong[2], SU Dongxu[2], and JIN Lina[2]

1 *Key Laboratory of Marine Sedimentology and Environmental Geology, First Institute of Oceanography, State Oceanic Administration, Qingdao, Shandong 266061, China*
2 *School of Energy Resources, China University of Geosciences (Beijing), Beijing 100083, China*
3 *Research Institute of Shaanxi Yanchang petroleum (Group) company limited, Xian, 710065, China*
4 *Department of Geology and Geophysics, Louisiana State University, Baton Rouge 70803, USA*

Abstract: The Shan 2 Member, Shan 1 Member and He 8 Member of the Mid–Late Permian Shanxi and lower Xiashihezi formations, in the southeastern Ordos Basin, together comprise ~150 m of deltaic deposits. This sequence records an overall evolution from deep marine environment to shallow lake associated with braided river, braided river delta and meandering river delta. Core description, well log interpretation, and stable isotope analysis, including carbon, oxygen and strontium, were conducted to understand the sedimentary evolution of Shan 2 to He 8 Member. The Shanxi Formation, which consists of the Shan 2 and Shan 1 members, is characterized by a tidal-influenced meandering river delta environment and a higher δ^{13}C value and $^{87}Sr/^{86}Sr$ ratio and a lower δ^{18}O value. The He 8 Member, the basal part of the Xiashihezi Formation, is featured by a braided river to braided river delta system and a lower δ^{13}C value, $^{87}Sr/^{86}Sr$ ratio, and a higher δ^{18}O value. Four third-order depositional sequences separated by five sequence boundaries are determined. Coarsening upward sequences of the Shan 2 Member–He 8 Member indicate a general regression trend, which can be correlated to global sea-level fall occurring during the Roadian–Wuchiapingian, as also evidenced by previous published zircon U–Pb results. The coal-bearing sequence (Shanxi Formation) to non-coal-bearing sequence (He 8 Member), as well as a decrease of $^{87}Sr/^{86}Sr$, suggest a trend from humid to arid climates. A combined effect of sea-level drop and a small uplift at the end of Shanxi Formation are proposed.

Key words: sequence stratigraphy, sedimentary sequence, delta, marine to lacustrine evolution, Roadian –Wuchiapingian, Ordos Basin

1 Introduction

The Ordos Basin is a craton basin developed on North China Block (Yang et al., 2005a), with a normal sediment thickness less than 6 km (Xiao et al., 2005). The craton basin records a long-term depositional history, reflecting the interplay between sediment supply and accommodation space. With a prolonged and low subsidence rate, the craton basin fill is characterized by predominantly shallow water and terrestrial sedimentation (Allen and Allen, 2013). Many petroleum and gas plays are genetically related to coastal and shallow water settings (Catuneanu, 2006), especially for deltas, which are good places for oil and gas to accumulate (Beglinger et al., 2012). Delta environments are shaped by sediment input and basinal reworking processes. Understanding these processes and products are crucial, and represent a critical prerequisite for predicting oil and gas reservoir distribution.

The Ordos basin experiences a long subsidence duration from Middle Cambrian to Middle Jurassic (Hu et al., 2013). A 12–18 m Myr^{-1} sediment accumulation rate in this basin is extremely low compared to surrounding rift basins, i.e. Erlian and Bohai Bay basins. During the

* Corresponding author. E-mail: xshan@fio.org.cn; billyu@cugb.edu.cn

Pennsylvanian, the basin experienced a large-scale transgression and deposited the Benxi Formation and Taiyuan Formation (Li et al., 2008), with sedimentary environments characterized by barrier islands, extensive tidal flats and shallow marine facies with some limited deltaic deposition in northern parts (Xiao et al., 2005; Yang et al., 2005a). The succeeding lower Permian Shanxi Formation and basal part of the Xiashihezi Formation (He 8 Member), which consist of fluvial-deltaic clastic rocks, were deposited in a regression background based on sedimentological analysis (Zhu et al., 2008). Comprising the Shan 2 Member and Shan 1 Member, the Shanxi Formation consists of several coal seams, which indicate warm and humid marginal marine environments (Zhu et al., 2008). Marine organisms such as Foraminifera and brachiopods *Dictyoclostus taiyuanfuensis* and *Compressoproductus mongolicus* were identified in the Shan 2 member (Lower Shanxi Formation) (Liu et al., 2006a). The He 8 Member is characterized by thick-bedded sandstone (Chen et al., 2011; Tian et al., 2011). A consensus is agreed that the overlying He 7 Member–He 5 Member (upper Xiashihezi Formation) were deposited in a fluvial-lacustrine setting (continental facies) (Tian et al., 2011). As a result, the Shanxi Formation and He 8 Member provide an exceptionally complete and well-preserved depositional record of a marine to lacustrine evolution in a craton basin. Conducting sedimentological and sequence stratigraphic study on this depositional record is thus important for understanding marine to lacustrine evolution in a craton basin.

The idea that "oil exists in the southern part of the Ordos Basin, and gas accumulates in the northern part" has prevailed for a long time (Wang, 2014). Conventional studies suggested that deep-water facies dominated by fine-grained sediments developed in the study area (Hu et al., 2010; Yang et al., 2005b), and thus reservoirs for gas accumulation cannot be found in the Paleozoic strata in the southeastern Ordos Basin. Our study clearly indicates that in the Shan 2 Member–He 8 Member, the sedimentary environments are deltas that could provide potential reservoirs for gas accumulation.

In this paper, the sedimentology and sequence stratigraphy of the Shan 2, Shan 1 and He 8 members are researched. We also provide the first reported carbon (C), oxygen (O), and strontium (Sr) isotopic results from this extraordinary stratigraphic section to increase understanding of the marine to lacustrine deltaic evolution.

2 Geological Background

The Ordos basin is floored by a double-layer basement: a lower layer of Archean igneous and metamorphic rocks and an upper layer of Lower Proterozoic metamorphic rocks (Yang et al., 2005a; Hu et al., 2013). Having an area of 320,000 km^2, the Ordos basin is oval in shape with a lack of widespread extensional faults (Fig. 1). The crust thickness is about 40–45 km (Liu et al., 2006b). The basin can be subdivided into six structural units comprising the Western Edge Fault Belt, Tianhuan Depression, Yishan Slope, Jinxi Fold-Fault Belt, Yimeng Uplift, and Weibei Uplift (Fig. 2a).

The basin evolution experiences four stages, comprising Cambrian–Early Ordovician continental rim basin, Middle Ordovician to Middle Triassic Craton Basin with convergent margins, Middle Ordovician–Middle Triassic Craton Basin with divergent margins, and Late Triassic–Early Cretaceous intraplate remnant craton basin. The stratigraphy consists of Lower Paleozoic, Upper Paleozoic and Mesozoic rocks (Fig. 1d), with a sediment thickness of 4000–6000 m (Xiao et al., 2005). During the late Paleozoic, the Yin Mountains were uplifted in the northern part of the basin, becoming the main sediment source (Yin and Harrison, 1996). The Qinling mountain belt in the south of the basin might also have been a potential source area for the Ordos area during the Pennsylvanian to Permian, because the Qinling range separates the North and South China cratons, and the first collision between these two cratons was in the Devonian (Mattauer et al., 1985).

Six lithostratigraphic formations including the Benxi Formation, Taiyuan Formation, Shanxi Formation, Xiashihezi Formation, Shangshihezi Formation and Shiqianfeng Formation constitute the Upper Paleozoic Pennsylvanian–Permian succession (Fig. 2b). In this period, the Ordos basin underwent a huge sedimentary environmental change from marine environments i.e. barrier-lagoon system in the Benxi Formation to continental, i.e. fluvial and floodplain in the Shangshihezi Formation. During the Benxi period, the sedimentary environment is characterized by a barrier-lagoon system along a paleo-uplift in the central basin. Due to a transgression in the Taiyuan period, a carbonate platform dominated in the central basin, with some alluvial fans developed along the Yin Mountains in the north. The basin experienced an overall regression from the Taiyuan period to the Shiqianfeng Formation. The Permian Shanxi Formation, which can be divided into two members, the Shan 2 Member at the base and the Shan 1 Member above, has a thickness of 100–130 m. The succeeding He 8 member, having a thickness of ~50 m, is also characterized by fluvial-deltaic deposits.

The Ordos Basin, located in the western part of the North China Craton, was influenced by the Paleo-Asian Sea, the Mianlue Sea, and the Shangdan Ocean during

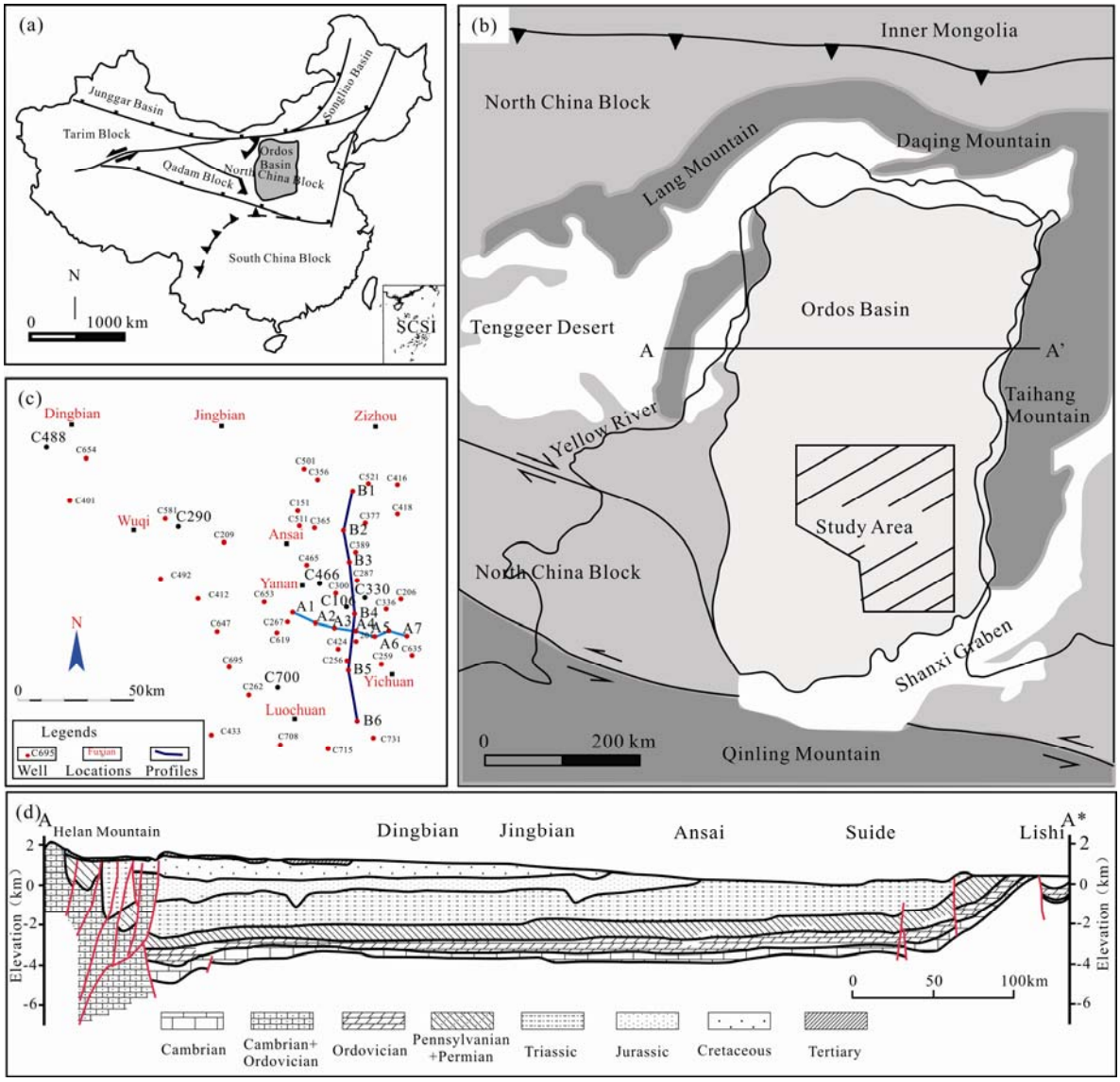

Fig. 1. Study site and location.
(a), The Ordos Basin is on the western part of the North China Block; (b), the study area is in the southeast Ordos Basin; (c), well and profile locations; (d), A-A' profile taken from the middle part of the Ordos Basin (modified from Yang et al., 2005a).

Late Paleozoic (Fig. 2c) (Li et al. 2017b). The Carboniferous to Permian experienced a drastic climate change from icehouse to greenhouse conditions (Nakazawa et al., 2015).

3 Methods

The outcrop of Shan 2 Member, Shan 1 Member and He 8 Member was measured in the Lvliangshan area. Core from 46 wells, with a total thickness of 1949 m, located in the Yan'an Core Laboratory, Yan'an City, Shaanxi Province, were described to identify sedimentary textures (color, grainsize, rounding, and sorting) and sedimentary structures. A detailed stratigraphic analysis was conducted on cores, outcrop and well-log curves, and samples were collected at 5–10 m intervals for petrography and geochemistry analysis.

Carbon and oxygen isotopic compositions of sedimentary carbonates in mudstone, and Sr isotopic compositions of mudrocks were determined and are used to infer climate change, relative sea-level change and further tectonic evolution throughout the Ordos basin.

As the study area is ~6×10^4 km^2, 32 samples of mudstone from 10 wells were averagely distributed in the southeast Ordos Basin and evenly selected from the Shan 2 Member, Shan 1 Member and He 8 Member for isotopic analysis. As a result, a detailed analysis of chemo-stratigraphy for a single sedimentary sequence was not possible. Obvious secondary fabrics including bioturbations, recrystallization, replacement, and fractures were avoided. These samples were analyzed at the Institute of Soil Science, Chinese Academy of Science,

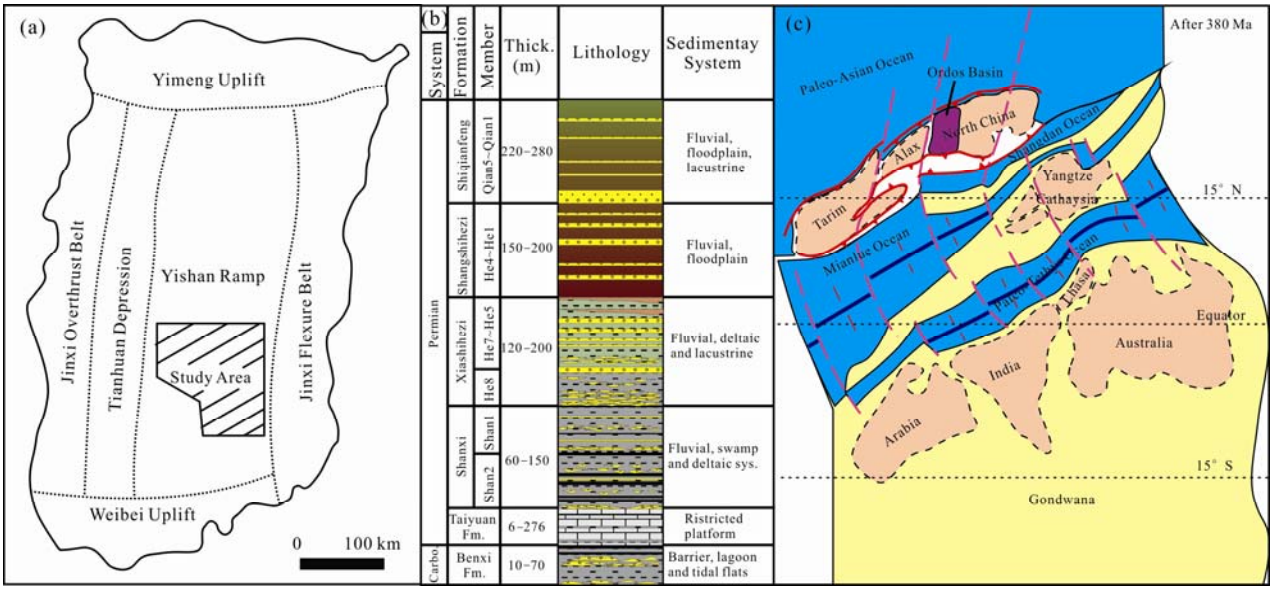

Fig. 2. Geological setting of Ordos Basin.
(a), Tectonic subdivision of the Ordos Basin, with the study area highlighted; (b), Upper Paleozoic stratigraphy of the Ordos Basin; (c), location of the Ordos Basin and North China Block after 380 Ma (modified from Li et al., 2017 in press). Note that the Ordos Basin might have been influenced by the Paleo-Asian Sea and the Shangdan Sea.

Nanjing, China.

For C and O isotopes of sedimentary carbonate of mudstone, between 0.5 and 1 mg of each sample was reacted with orthophophoric acid in a Kiel IV carbonate device connected to a MAT 253 manufactured by Finnigan. Strontium isotopes ^{86}Sr and ^{87}Sr were determined using a Triton TIMS (Finnigan). The detailed pre-treatment steps can be found in Li et al. (2011) and Wang et al. (2014).

4 Facies Analysis and Paleoenvironmental Interpretation

Core-based lithofacies have been identified using the lithofacies classification scheme proposed by Miall (1988). The Shan 2 Member, Shan 1 Member and He 8 Member in southeastern Ordos Basin together comprise 19 types of lithofacies (summarized in Table 1 and see Fig. 3). These lithofacies are interpreted as having formed in environments ranging from non-marine (fluvial and lacustrine delta) to marine coastal settings (deltaic and tide -influenced system). Based on core and field observations, two facies associations can be distinguished: (1) tide-influenced meandering river delta; and (2) braided river and braided river delta.

4.1 Facies association 1 – Tide-influenced meandering river delta facies

This facies association features thick-bedded mudstone, which can be more than 10 m thick, interbedded with thin- to medium-bedded fine- to medium-grained sandstone. In the sandstone, trough cross bedding, tabular cross bedding, parallel bedding and wave ripples can be identified (Table 1). In the basal part, channel-shaped sandstone deeply incises the underlying carbonate of the Taiyuan Formation in the northeast of the study area (Fig. 4a). Flaser bedding, wavy bedding and lenticular bedding can be easily found in the core (Fig. 4e and 4g), especially in the central area of the study area. Coal seams, with a thickness of ~0.2–0.5 m, are very common (Fig. 4b and 4f). Muscovite is very rich along the bedding surfaces of the sandstone, and sometimes in the mudstone (Fig. 4h). A variety of fossil plants are buried in the dark black mudstone (Fig. 3j). Mud clasts in the Shanxi Formation are angular to sub-angular. The Shan 2 Member and Shan 1 Member have these typical features.

The channel-shaped sandstones, as well as the trough, tabular cross bedding, and parallel beddings, are clearly indicators of unidirectional flow. Angular mud clasts are usually associated with meandering channels, and these clasts are formed by channel lateral incision (Li et al., 2017a). Besides these alluvial features, the association of flaser bedding, wavy bedding and lenticular bedding are typical tidal markers. Tidal rhythmites, small-scale sedimentary structures including mud drapes, bidirectional flow ripples identified in the core also suggest tidal influence (Fig. 4g). Wave influence in the Shanxi Formation is evidenced by the presence of wave-dominated sediments including beach deposits featured by swash laminated sandstone (Fig. 4c), as well as a mouth bar deposit characterized by multiple sets of planar cross bedded and wave rippled sandstones (Fig. 4d–e). The

Table 1 Lithofacies summary of Shan 2 Member – He 8 Member

Number	Code	Lithofacies name	Lithology	Sedimentary textures	Sedimentary structures	Interpretation
1	Gm	Poorly sorted, matrix-supported conglomerates	From fine sandstone to cobble size conglomerate. The largest grain size is 3.4 cm.	Poorly sorted. Bimodal. Sub-rounded.	Matrix supported	
2	Gt	Trough cross-bedded conglomerates	From medium grained to pebble sized conglomerate. The largest grain size is 1.2 cm.	Moderate sorted. Sub-rounded to sub-angular.	Trough cross bedding. Fining upward trend.	Sinuous crested dunes and 3-D transportation. Lower flow regime.
3	Gp	Planar cross-bedded conglomerates	From coarse grained to pebble sized conglomerate. The largest grain size is 1.5 cm.	Moderately sorted. Sub-rounded.	Planar cross bedding. Coarsening upward trend.	Straight crested dunes and 2-D transportation. Lower flow regime.
4	Gmm	Poorly sorted, matrix-supported mudclasts	From coarse grained to cobble sized conglomerate. The largest grain size is 6.8 cm.	Poorly sorted. Sub-angular to angular.	Matrix supported	Meandering style channel. Outer bank insicion. Collapse origin.
5	Gmi	Imbricated mudclasts	From medium grained sandstone to pebble sized conglomerate. The largest grain size is 1.4 cm.	Moderately sorted. Sub-rounded.	Clast supported	Long distance transportation origin.
6	Gi	Imbricated conglomerates	From granule to pebble sized conglomerate. The largest grain size is 2.8 cm.	Poorly sorted. Sub-rounded to sub-angular.	Gravel imbrication	Bedload and tractive current. Typical fluvial deposits.
7	St	Trough cross-bedded sandstone	Fine to conglomeratic coarse grained sandstone.	Moderately sorted.	Trough cross bedding. Fining upward trend.	Sinuous crested dunes and 3-D transportation. Lower flow regime.
8	Sp	Planar cross-bedded sandstone	Fine to coarse grained sandstone.	Moderately well sorted.	Planar cross bedding. Coarsening upward trend.	Straight crested dunes and 2-D transportation. Lower flow regime.
9	Sh	Horizontal bedded sandstone	Fine to medium grained sandstone.	Moderately well sorted.	Horizontal bedding	Upper flow regime.
10	Sr	Ripples cross laminated sandstone	Silty fine to medium grained sandstone.	Moderately well sorted.	Unidirectional current ripples.	Unidirectional flow. Lower flow regime.
11	Swr	Wave rippled sandstone	Silty fine to medium grained sandstone.	Well sorted.	Wave ripples.	Bidirectional current ripples.
12	Sf	Flaser bedded sandstone	Fine grained sandstone.	Moderately well sorted.	Flaser bedding.	Tidal current. High current speed. Low preservation of mud drapes.
13	Sw	Wavy bedded sandstone	Fine to medium grained sandstone.	Moderately well sorted.	Wavy bedding.	Tidal current. Medium current speed. Midum preservation of mud drapes.
14	Sl	Lenticular bedded sandstone	Siltstone to fine grained sandstone	Moderately well sorted.	Lenticular bedding.	Tidal current. Low current speed. High preservation of mud drapes.
15	M	Mudstone	Claystone or/and silty mudstone	Moderately sorted.	Massive.	Deposition from suspension.
16	Mp	Plant debris bearing mudstone	Claystone	Moderately sorted.	Plant debris.	In situ deposition.
17	Mm	Muscovite mudstone	Claystone	Moderately sorted.	Muscovite.	In situ deposition. Short distance to the river mouth.
18	Mpm	Plant debris and muscovite bearing mudstone	Claystone	Moderately sorted.	Plant debris and muscovite.	In situ deposition.
19	C	Coal	Coal			Vegetated swamp or tidal flat deposits.

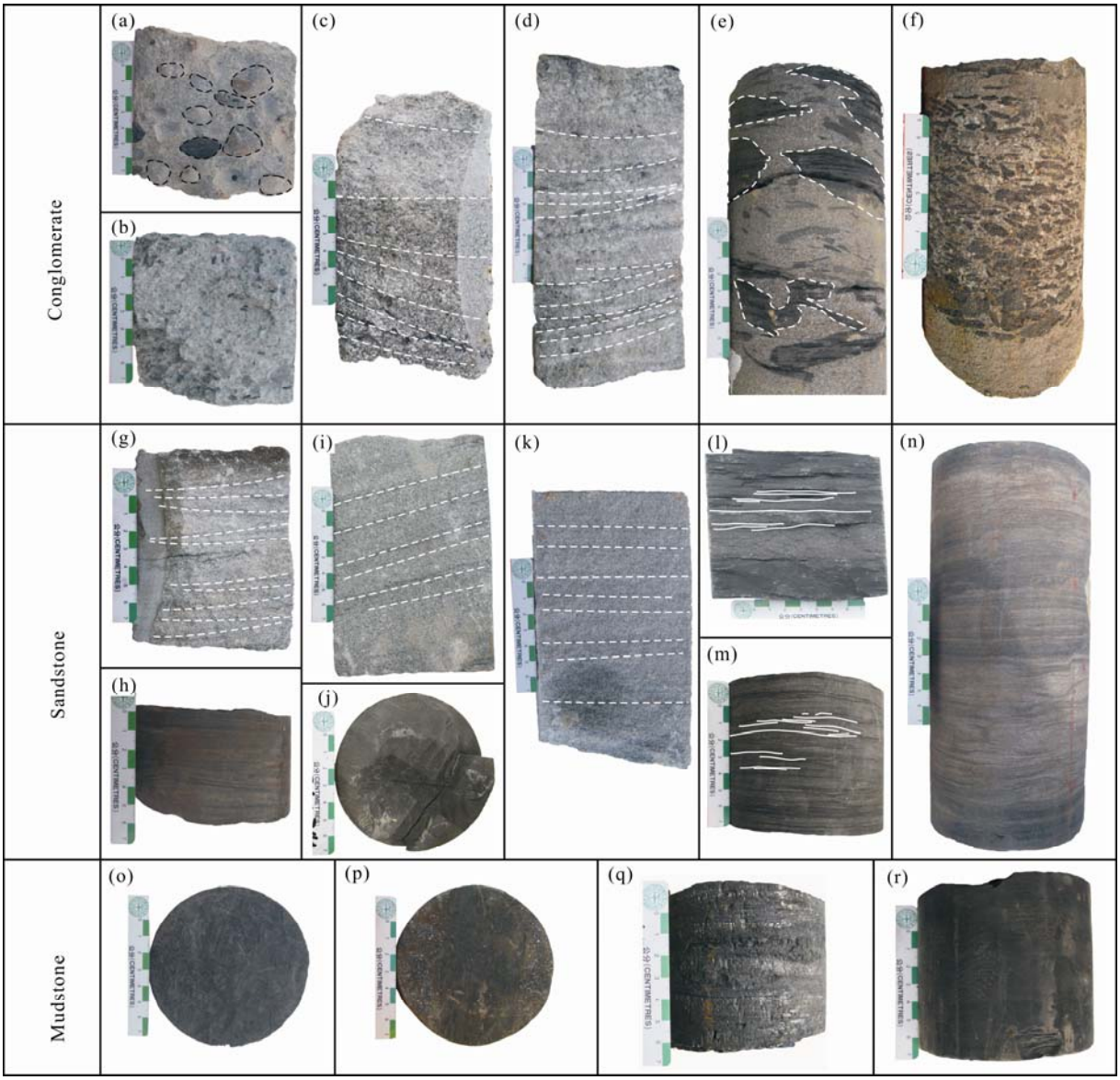

Fig. 3. Core photographs of lithofacies.

(a), Poorly sorted medium-grained sandstone to pebble-sized conglomerate, He 8 Member. Well C700, 2804.37 m; (b), coarse-grained sandstone to pebble with imbrication, He 8 Member, Well C498, 3053.94 m; (c), gray planar cross-bedded pebble-sized conglomerate, He 8 Member, Well C488, 3891.83 m; (d), gray trough cross-bedded granule to pebble-sized conglomerate, Shan 1 Member, Well C488, 3898.66 m; (e), poorly sorted and angular mud clasts, which indicate an erosion of the outer bank and meandering-style origin in the Shan 1 Member. Well C290, 3944.25 m; (f), moderate to well-sorted and rounded mudclasts, which indicate a long-distance transportation genesis identified in the He 8 Member, Well C635, 2202.35 m; (g), trough cross-bedded sandstone, Shan 1 Member, Well C492, 3951.93 m; (h), rippled cross-laminated sandstone, Shan 2 Member, Well C412, 3510.93 m; (i), planar cross-bedded sandstone, He 8 Member, Well C488, 3918.77 m; (j), fine-grained sandstone with plant fossil *Pecopteris fuyuanensis*, He 8 Member. Well C521, 2455.47 m; (k), horizontal-bedded sandstone, Shan 1 Member, Well C465, 2927.83 m; (l, m), wave -rippled fine-grained sandstone, Shan 2 Member and Shan 1 Member. Note the symmetrical shape, Well C336, 2513.11 m and 2514.21 m; (n), tidal rhythmites, Shan 1 Member, Well C581, 3960.01 m; (o), black claystone with plant fossil *Sphenopteridium pseudogermanicum*, Shan 2 Member, Well 356, 3076.24 m; (p), muscovite siltstone with plant fossil *Calamites suckowii*, Shan 1 Member, Well C106, 2788.96.04 m; (q), coal, Shan 2 Member, Well C356, 3073.99 m; (r), massive claystone, Shan 1 Member, Well C287, 2611.86 m.

muscovite sandstone type of the Shanxi Formation can be explained by an environment of unloading and dumping. The well-developed coal seams suggest a low-energy setting, and humid and warm climate. As a result, based on identifications of meandering channel, mouth bar deposits, tidal markers, and the low energy setting, we propose that the facies association described here is formed by a tide-influenced meandering river delta.

4.2 Facies association 2 – Braided river and braided river delta

In the southeastern Ordos Basin, the facies association is characterized by thick-bedded (usually >15 m) conglomeratic medium- to coarse-grained sandstone intercalated with thin- to medium-bedded mudstone. In the thick-bedded sandstone, multiple channel-shaped sandstone can be identified (Fig. 5a −b). The grain size is

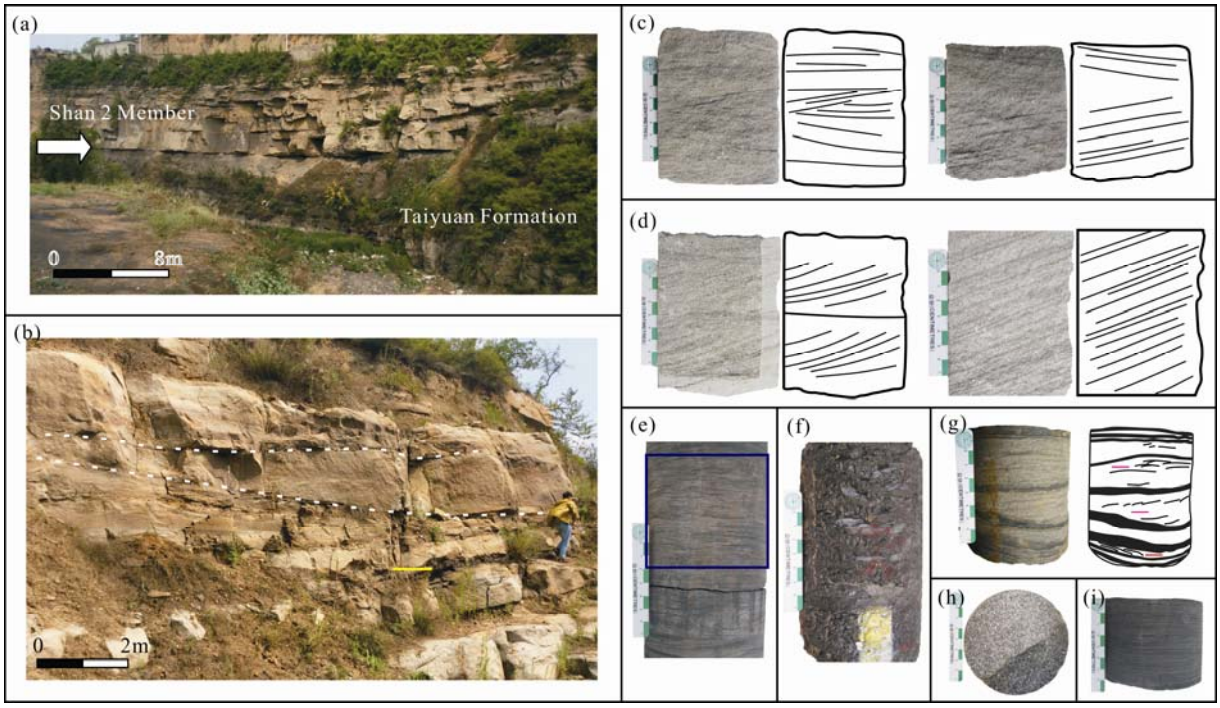

Fig. 4. Sedimentary characteristics of the meandering river delta of the Shanxi Formation.
(a), Unconformity (white arrow) at the contact between the Shan 2 Member, Shanxi Formation and Taiyuan Formation. The lower Shan 2 Member features fining-upward fluvial sedimentary rocks, whereas the Taiyuan Formation is dominated by carbonates; (b), thick-bedded (>3m) fluvial channel scoured into underlying thin-bedded distributary channels, which indicates an increase in sediment supply from the Shan 1 Member. Note the presence of coal (yellow arrow) deposited in a low energy setting (inter-distributary area); (c), swash cross-bedded sandstone formed by swash and backwash processes on the foreshore, Shan 1 Member. (d), planar cross-bedding, Shan 1 Member. Note the multiple sets of planar cross-bedded sands, which are interpreted as mouth bar deposits; (e), wave-modified symmetric ripples in fine-grained sandstone, Shan 2 Member; (f), black coal deposits formed in a low energy setting, Shan 2 Member; (g), ripple cross-lamination, Shan 1 Member. Red arrow shows cross-lamination dipping right, purple arrows show lamination dipping left. Note the mud drapes between laminations. Reversing flow directions with mud drapes indicate tidal influence; (h), fine-grained sandstone comprises predominantly muscovite, which is interpreted as deposited in an area near river mouth, Shan 1 Member; (i), lenticular bedding, which indicates tidal influence, Shan 1 Member.

much coarser than in facies association 1. The conglomerate bed thickness and the maximum gravel size decreases towards the central area. Large-scale trough and planar cross beddings are common (Fig. 5a−c). Wave ripples can be identified in the core (Fig. 5d). Coal seams are rare in this association. The mud clasts display rounded to sub-rounded shape (Fig. 3f).

The thick-bedded sandstone with multiple channels is a closely stacked braided river channel deposit. The hydrodynamic condition is stronger than in facies association 1, because of the large scale of sedimentary structures, and the absence of low-energy settings which can generate coal seams. The rounded to sub-rounded mud clasts indicate that they have been transported. The lithofacies association of cross-bedded (trough and planar) granule-sized conglomerates, cross-bedded sandstones and wave-rippled sandstone suggests that these deposits formed in a braided river delta environment, which can be subdivided into braided delta plain, delta front and prodelta. The delta plain is dominated by braided channel and braided bar deposits. The gravelly and sandy braided river channels show an overall fining-upward trend. The braided bar deposits display a coarsening-upward sequence featuring large-scale multiple sets of trough and planar cross bedding (Fig. 5a). The delta front deposits mainly comprise sandy/gravelly river mouth bars and distal bars. The dark gray to black mudstone, without signatures of fluvial and basin reworking processes (wave and tide), formed in a prodelta.

4.3 Sedimentary sequences of genetic units

Based on the detailed core description, six typical sedimentary sequences are identified in the Shan 2 Member, Shan 1 Member and He 8 Member, representing different genetic units. They comprise meandering channel sequence (Fig. 6a), river mouth bar with insufficient sediment supply (Fig. 6b), tidal flat (Fig. 6c), braided channel and braided bar sequence (Fig. 6d), which represent upper braided delta plain, braided channel, and river mouth bar deposits (Fig. 6e), which represent lower delta plain, and river mouth bar with sufficient sediment supply (Fig. 6f).

The meandering channel, river mouth bar with insufficient sediment supply and tidal flat mainly form in a meandering river delta system (Shan 2 Member and Shan 1 Member). Braided channel, braided bar and river mouth

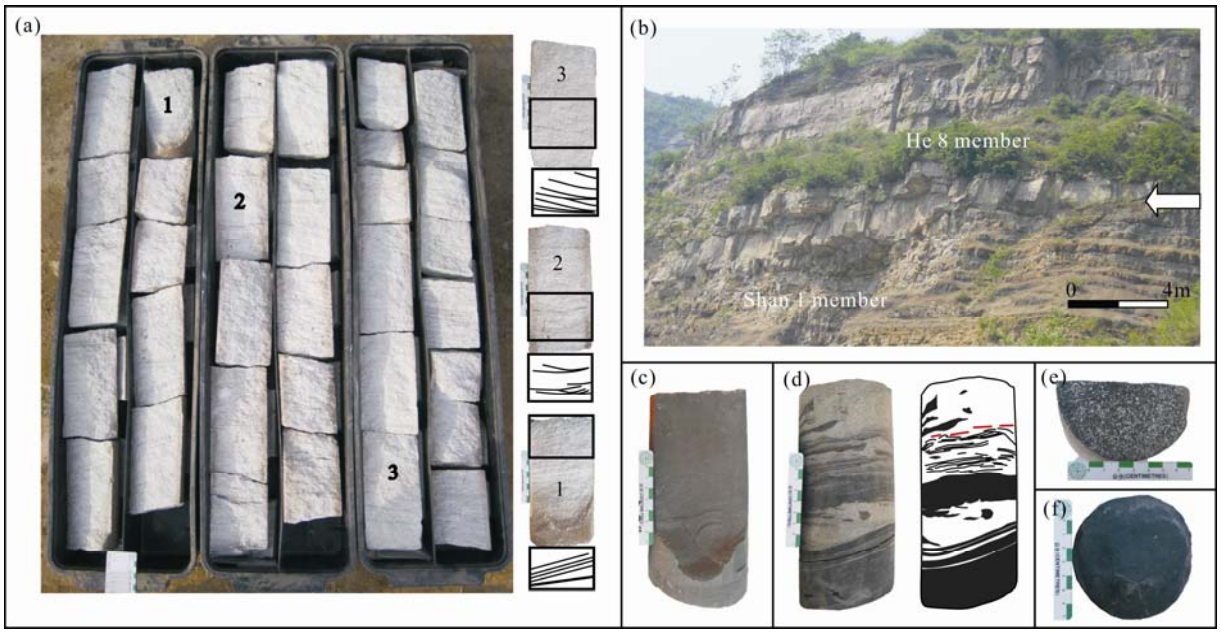

Fig. 5. Sedimentary characteristics of the braided river delta of the He 8 Member.
(a), Fluvial sandstone represented by thick-bedded conglomeratic coarse-grained sandstone. Note the presence of alternating planar cross-bedding and trough cross-bedding; (b), unconformity (arrowed) at the contact between the Shan 1 member (Shanxi Formation) and the overlying He 8 Member (Xiashihezi Formation). The succession of the Shan 1 Member is overbank fines and thin-bedded (<1 m) sandstones, with an abrupt increase in energy levels across the contact. Note the change from thin-bedded sandstone to amalgamated braided channels; (c), gray silt to fine-grained sandstone with no obvious sedimentary structures, interpreted to form in a subaqueous environment; (d), wave-modified ripples in heterolithic beds. Note the opposite lamina dips and rounded ripple troughs; (e), wave-modified ripples in heterolithic beds. Note the opposite lamina dips and rounded ripple troughs.

bar with sufficient sediment supply form in a braided river delta system (He 8 Member).

5 Stable Isotope Results

A complete carbon, oxygen and $^{87}Sr/^{86}Sr$ record is shown in Figure 7a–b. $\delta^{18}O$ is more prone to suffer diagenetic alteration, and care must be taken when interpreting the data (Gomez et al., 2007). $\delta^{13}C$, $\delta^{18}O$ and $^{87}Sr/^{86}Sr$ are analyzed in the study (Table 2).

The $\delta^{13}C$ values fluctuate between −3.7‰ and −0.5‰ and the $\delta^{18}O$ between −9.6‰ and −4.6‰ relative to the VPDB standard (Fig. 7a). The Shan 2 Member shows a stable pattern, with $\delta^{13}C$ values ranging from −3.3‰ to −0.7‰ (mean value −1.8‰) and $\delta^{18}O$ values from −8.6‰ to −5.0‰ (mean value −7.5‰). In the Shan 1 Member, $\delta^{13}C$ ranges from −3.6‰ to −0.5‰ (mean value −1.9‰), and $\delta^{18}O$ shows more negative values from −9.0‰ to −5.8‰ (mean value −8.0‰). The He 8 Member $\delta^{13}C$ values become more negative from −3.7‰ to −0.5‰ and the mean value is −2.0‰. A more positive $\delta^{18}O$ value of −4.6‰ is recorded in the He 8 Member, with a mean value of −7.3‰.

$^{87}Sr/^{86}Sr$ values of the Shan 2, Shan 1 and He 8 Members are from the mudstone in 10 wells. The $^{87}Sr/^{86}Sr$ values range from 0.7174 to 0.7374, with a mean value of 0.7275 (Fig. 7b). The $^{87}Sr/^{86}Sr$ of the Shan 2 Member shows values from 0.7217 to 0.7374, with a mean value of 0.7285. The $^{87}Sr/^{86}Sr$ values of the Shan 1 Member show a similar pattern compared with the Shan 2 Member with a mean value of 0.7290. The $^{87}Sr/^{86}Sr$ of the He 8 Member shows lowest values from 0.7174 to 0.7315, with a mean value of 0.7260.

6 Sequence Stratigraphy Analysis

On the Yishan slope in the southeastern Ordos Basin, the Shan 2 Member, Shan 1 Member and He 8 Member show the most complete stratigraphic record. It can be utilized for sequence stratigraphic analysis.

6.1 Sequence boundaries and bounding surfaces

Recognition of the sequence boundary in alluvial strata can be difficult, because basinward shift and related incision can easily be confused with local channel scour (Flint et al., 1995). Sequence boundaries can be identified by numerous features such as abrupt increase in vertical sandstone amalgamation and an increase in mean grain size and sandstone composition change (Dapples, 1947; Schumm, 1993). Sequence boundaries recognized in this study are erosional or non-depositional surfaces created during base level fall by fluvial incision or pedogenesis (Catuneanu, 2006). These surfaces separate strata that are genetically unrelated, and mark abrupt basinward shift

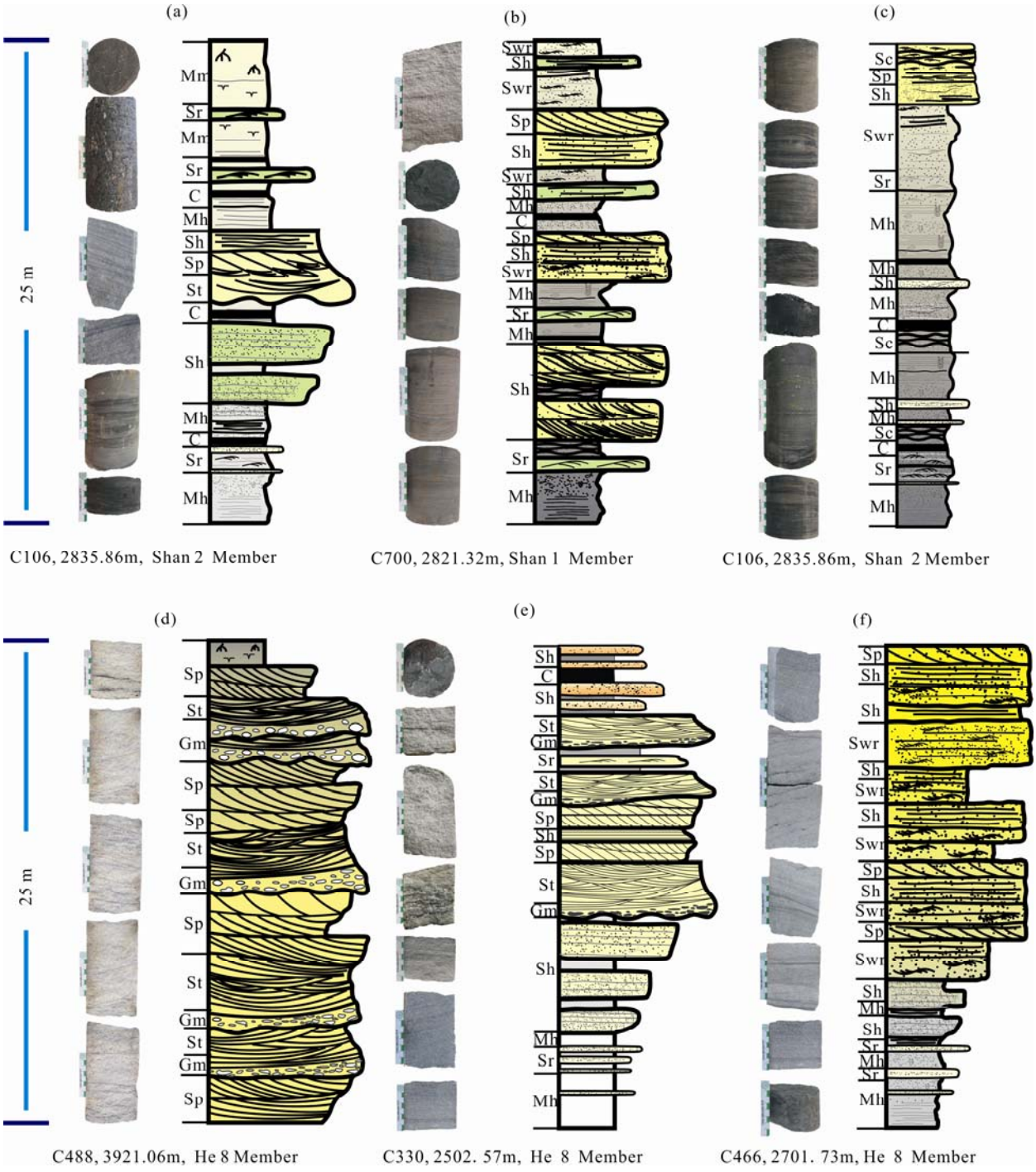

Fig. 6. Six summarized sedimentary sequences of genetic units.
(a), Meandering channel sequence; (b), river mouth bar with insufficient sediment supply. Note the planar cross-bedding and parallel bedding representing wave process and tidal rhythmites representing tidal influence; (c) tidal flat deposits; (d), braided channel and braided bar sequence representing upper braided delta plain; (e), braided channel and river mouth bar deposits representing lower delta plain. Note the presence of mud clasts at the channel base; (f) river mouth bar with sufficient sediment supply. The wells and depths are indicated.

(Catuneanu et al., 2011).

Sandstone amalgamation at the base of the Shanxi Formation and an abrupt change in petrographic composition from the limestone of the Taiyuan Formation to the coal-bearing sequence of the Shanxi Formation indicate a sequence boundary (Fig. 4a). The incision depth is 8–15 m. The other sequence boundaries identified in this study are in the Shanxi Formation. They feature river mouth bar deposits or beach swash laminated sandstone or deep sea mudstone incised by deltaic channel, which show a facies discontinuity and relative sea-level drop (Fig. 8a–c).

The He 8 Member is a clastic wedge derived from both the Yin mountains to the north and the Qinling Mountains

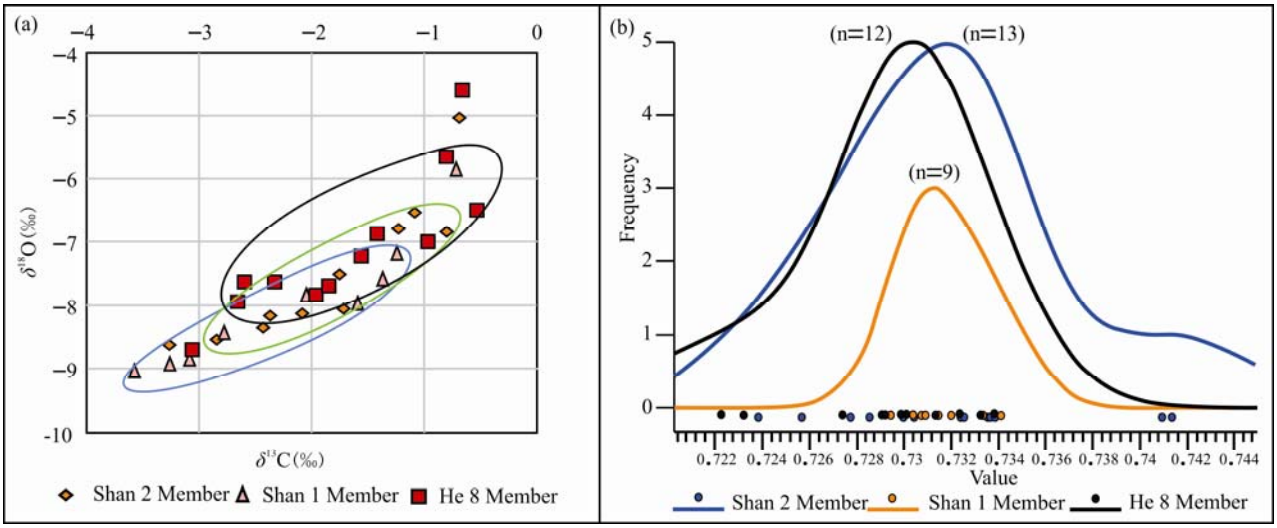

Fig. 7. Stable isotopes of the Shan 2 Member–He 8 Member.
(a), Carbon versus oxygen isotope plots from all 10 wells; (b), $^{87}Sr/^{86}Sr$ ratios of the three members.

Table 2 Carbon, oxygen, and Sr^{87}/Sr^{86} isotope of Shan 2 Member – He 8 Member

Num	Strata	Well	$\delta^{13}C_{PDB}$(‰)	$\delta^{18}O_{PDB}$(‰)	Sr^{87}/Sr^{86}	Num	Strata	Well	$\delta^{13}C_{PDB}$(‰)	$\delta^{18}O_{PDB}$(‰)	Sr^{87}/Sr^{86}
1	He 8	c209	−0.52	−6.5	0.728552	17	He 8	c492	−1.84	−7.69	0.730877
2	Shan 1	c209	−1.24	−7.15	0.727655	18	Shan 2	c492	−1.75	−7.5	0.726428
3	Shan 2	c209	−0.8	−6.84	0.724549	19	Shan 2	c492	−2.08	−8.12	0.728536
4	He 8	c259	−0.96	−7.01	0.726974	20	He 8	c498	−1.56	−7.24	0.723704
5	Shan 1	c259	−1.37	−7.56	0.731788	21	He 8	c498	−1.41	−6.87	0.729779
6	Shan 1	c259	−1.58	−7.97	0.731809	22	Shan 2	c498	−1.23	−6.79	0.721675
7	Shan 2	c259	−1.72	−8.05	0.729666	23	Shan 2	c498	−1.08	−6.53	0.723737
8	Shan 1	c262	−2.05	−7.82	0.737355	24	He 8	c521	−0.66	−4.6	0.717401
9	Shan 2	c262	−2.37	−8.16	0.725982	25	He 8	c521	−0.81	5.65	0.726739
10	Shan 2	c262	−2.43	−8.34	0.736915	26	Shan 1	c521	−0.72	−5.84	0.729194
11	He 8	c321	−3.05	−8.69	0.727312	27	Shan 2	c521	−0.69	−5.03	0.729574
12	Shan 2	c321	−3.26	−8.62	0.728411	28	He 8	c581	−3.71	−9.64	0.718560
13	He 8	c330	−2.65	−7.94	0.725910	29	Shan 1	c581	−3.26	−8.9	0.730860
14	He 8	c330	−2.59	−7.63	0.731532	30	Shan 1	c581	−3.57	−9.03	0.726076
15	Shan 1	c330	−2.78	−8.41	0.727878	31	Shan 1	c581	−3.08	−8.82	0.727217
16	He 8	c492	−1.96	−7.83	0.728552	32	Shan 2	c581	−2.84	−8.54	0.719828

to the south (Tian et al., 2011). Its truncation implies the presence of an unconformity. The presence of numerous braided channel scour surfaces at the base of the He 8 Member confirms the sequence boundary between the He 8 Member (Sequence 4) and the Shan 1 Member (Sequence 3) (Fig. 5b). The total depth of incision is about 16–20 m, and related to a significant base level fall. On top of the He 8 Member (Sequence 4), a subaerial unconformity characterized by a multi-storey sandstone representing a sequence boundary can be identified (Tian et al., 2011).

A Maximum Regressive Surface (MRS) marks the change from lowstand regression to a subsequent transgression stage and separates a prograding pattern below from a retrograding pattern above (Catuneanu, 2006). In contrast, a Maximum Flooding Surface (MFS) marks the end of marine/lacustrine transgression, and displays a change from transgression to highstand normal regression (Wang et al., 2011).

6.2 Depositional sequence stratigraphic framework

The sequence framework facilitates paleogeographic reconstruction and the prediction of facies and lithologies. It also provides a context within which to interpret the sedimentary evolution through time and space (Catuneanu et al., 2011). Sequences and their internal system tracts are defined by specific strata stacking patterns and distinctive boundaries.

Integration of well logs, cores, outcrop and published researches allowed a sequence-stratigraphic framework to be developed for the Shanxi Formation and the He 8 Member in the Ordos Basin. This framework incorporates the lithology-based stratigraphic columns.

A sequence unit is bounded by a sub-aerial unconformity and its correlative conformity. In this study, four depositional sequences (namely SQ1, SQ2, SQ3, and SQ4) are bounded by five distinctive erosional surfaces (Fig. 9). Based on their chrono-stratigraphic framework, they represent 3rd order sequences, with one sequence ranging between ~0.5–3 My (Vail et al., 1988).

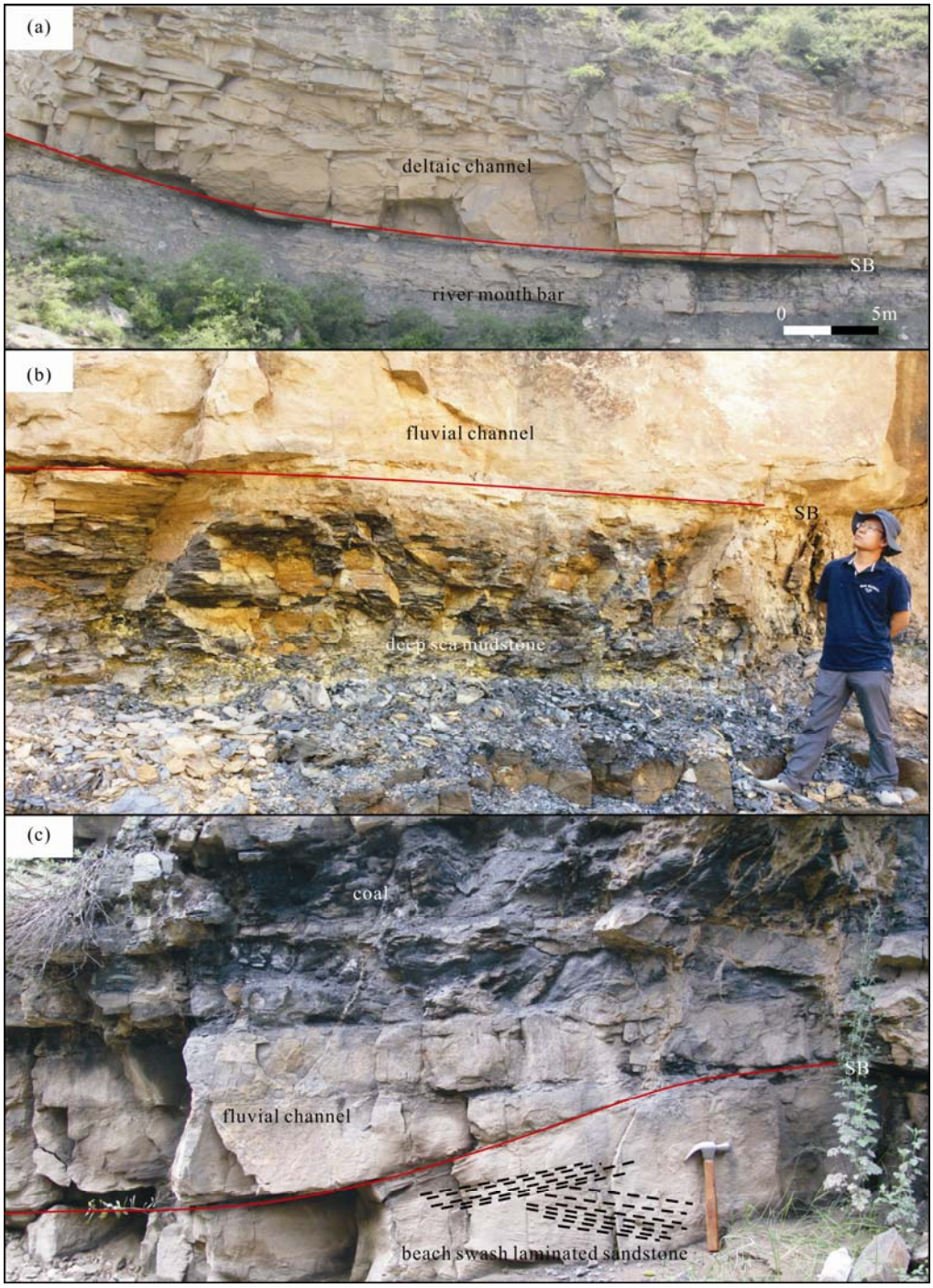

Fig. 8. Sequence boundaries.
(a), Mouth bar deposits incised by deltaic channels due to a base level fall; (b), deep marine dark blue mudstone eroded by a fluvial channel. Person for scale = 1.7 m high; (c) swash-laminated beach sandstone eroded by a fluvial channel indicating a facies discontinuity.

6.3 Sequence stratigraphic units

6.3.1 Sequence 1

Sequence 1 (SQ1) shows an average thickness of 20–40 m and is bounded by two sequence boundaries SB1 and SB2 at the base and top (Fig. 9). The sequence boundary SB 1 is well exposed at the section and is represented by a sharp boundary between oolitic limestone devoid of any siliciclastic material and decimeter-scale medium-coarse grained sandstones (Fig. 4a). The SB 1 surface occurs at the top of the *Triticites simplex* and *Pseudoschwagerina* biozones recorded within the Taiyuan Formation (Chao, 1925; Yuan, 1925). The large-scale cross-bedded fluvial or deltaic sandstones overlying SB 1 represent lowstand prograding wedge system tract deposits after the onset of sea-level rise (Fig. 4a). The overlying Transgressive System Tract (TST) is featured by coal development and

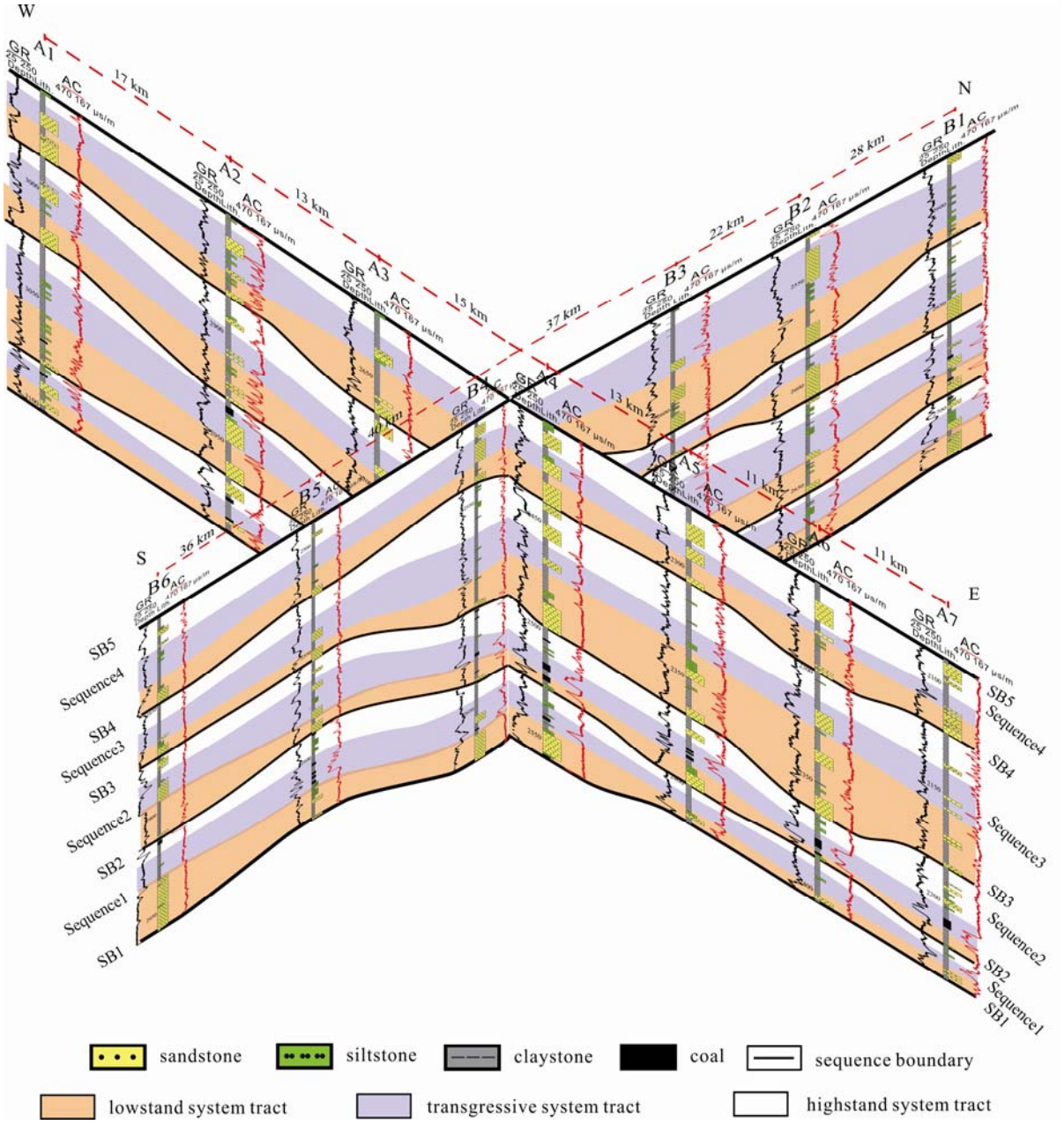

Fig. 9. Sequence stratigraphic framework of the Shan 2 Member–He 8 Member.
Four depositional sequences separated by five sequence boundaries for wells A1–A7 and B1–B6, the locations of which can be found on Fig. 1.

decreased coarse siliciclastic sediment input. The coal development in the TST was also suggested by Li et al. (2006) in the Upper Paleozoic Ordos Basin. The High System Tract (HST) shows a coarsening upward trend, although the sediment input is small compared with LST.

6.3.2 Sequence 2

Sequence 2 has an increased thickness (usually between 40–50 m), and occurs mostly in the middle part of the Shanxi Formation. In this sequence, coal is typically developed from the late LST to TST and constrained in the middle east and middle west of the study area (Fig. 8). Plant microfossils *Emplectopteridium alatum* Kaw and *Calamites suckowii* Brongniart are abundant in the sequence, which is consistent with the results of Wang (2010). The HST was partly eroded by the overlying lowstand prograding wedge, which can be identified in wells A2, A6 and B6 (Fig. 9), and which also explains a reduced thickness of HST in Sequence 2.

6.3.3 Sequence 3

The Sequence 3 has an average thickness of ~70 m. The lowermost sequence boundary SB 3 is an erosional surface truncating the underlying Sequence 2. This sequence

boundary is under the lowstand wedge units which developed at the middle west of the study area, and reflected by an increased thickness of LST deposits. Compared with Sequences 1 and 2, coal is less developed and the Sequence is much thicker, indicating an increase of sediment supply

6.3.4 Sequence 4

Having a thickness of ~35 m, Sequence 4 is mostly developed in the He 8 Member. It starts with the development of the underlying sequence boundary SB 4. This boundary is outlined by a significant contrast between thin- to medium-bedded shallow marine meandering deltaic deposits of the Shan 1 Member and the overlying thick-bedded and amalgamated braided deltaic deposits of the He 8 Member (Fig. 5b). The SB 4 can be easily identified in the study area, as it reflects a drastic relative sea level fall and represents a sharp boundary between the gray sub-litharenite to white litharenite (Zhou et al., 2014). In this sequence, the deposits feature thick-bedded conglomeratic medium to coarse sandstone. Lowstand system tract deposits occupy nearly half of the whole sequence. An increased sediment supply in this period can be deduced.

7 Discussion

7.1 Depositional ages of Shan 2 Member – He 8 Member

The youngest U–Pb ages of zircon grains can be utilized to constrain maximum depositional ages of stratigraphic units (Dickinson and Gehrels, 2009a), not only for Precambrian strata (Jones et al., 2009), but also for the Phanerozoic (Dickinson and Gehrels, 2009b). In our study, the depositional ages of the Shan 2 Member to He 8 Member are mainly determined by this approach through using published zircon U–Pb chronology results (Ma et al., 2011; Sun et al., 2014).

In the North China Craton, the Permian is mainly composed of the Taiyuan, Shanxi, Xiashihezi and Shangshihezi formations, from the base to the top. Sun et al. (2014) did zircon dating in the Taiyuan Western Mountain section, which is considered to be the standard Upper Paleozoic section. The Jinci Sandstone is developed in the basal Taiyuan Formation. Zircon U–Pb dating of this sandstone yields 296 ± 4 Ma, suggesting that this part of the Taiyuan Formation is in the scope of the Permian (Fig. 10). The Qiligou Sandstone, in the upper part of Taiyuan Formation, shows zircon U–Pb ages of 271 ± 7 Ma, indicating that the succeeding Shanxi Formation is already in the Middle Permian (Sun et al., 2014) (Fig. 10).

(Ma et al., 2011) conducted his research on the Xiashihezi Formation in the Pingquan area, Hebei Province. The zircon U–Pb result from a sand layer in the lower Xiashihezi Formation yields an age of ~258 Ma (Ma et al., 2011). Based on the sequence stratigraphic analysis, this sandstone can be assigned to the top of the He 8 Member or the base of the He 7 Member, which can nicely constrain the end date of the He 8 Member. As a result, the depositional age of the Shan 2 Member to the He 8 Member is 271 ± 7 Ma to ~258 Ma. According to our study, the end of the Shanxi Formation is characterized by a large-scale and strong sea-level fall, evidenced by a thick bedded (>15 m), multiple channel stacked sandstone in the lower part of the He 8 Member (Fig. 4a). According to the global sea-level curve proposed by Haq and Schutter (2008), between 271 Ma and 258, the largest global sea level fall occurred at 260.4 Ma, which correlates well with the strong regression at the end of Shanxi Formation (Fig. 10). Thus, the suggested depositional age of the Shanxi Formation is 271 ± 7 Ma to 260.4 Ma and the age of the He 8 Member is just after 260.4 Ma to 258 Ma. Based on these results, we propose that the Shan 2 Member–He 8 Member spans ~13 Ma.

7.2 Shanxi Formation and He 8 Member sea-level history and sedimentary evolution

In the Late Carboniferous and Permian, the sea-level change curve derived from a tectonically stable North China Block is closer to the global eustatic fluctuations than those from other parts of the world (Izart et al., 2003). Although the subsidence rate of the basin still played an important role in controlling accommodation space, our results show that the general transgressive/regressive trend can be correlated to global sea-level change events.

Previous sequence stratigraphic studies regarding the Shanxi Formation in the Ordos Basin were conducted by Zhang et al. (1997), Zhu et al. (2008) and Chen et al. (2011). Zhang et al (1997) primarily interpreted the clastic sediments of the Shanxi Formation in the northwestern Ordos Basin as a braided, anastomosing and meandering fluvial facies association. Zhang et al (1997) also proposed that the whole Shanxi Formation is one single third-order depositional sequence, with braided sandstone in the lowstand system tract, anastomosing river in the transgressive and meandering river in the highstand. Considering the whole Shanxi Formation spans more than 10 Ma, we think that this interpretation is too broad in scale.

In the basin margin, which is proximal to the source area, more sequence boundaries can be identified (Catuneanu, 2006). According to Zhu et al (2008), the lower member of Shanxi Formation, which is the Shan 2 Member of our study, represents a second-order sequence and can be subdivided into three third-order sequences.

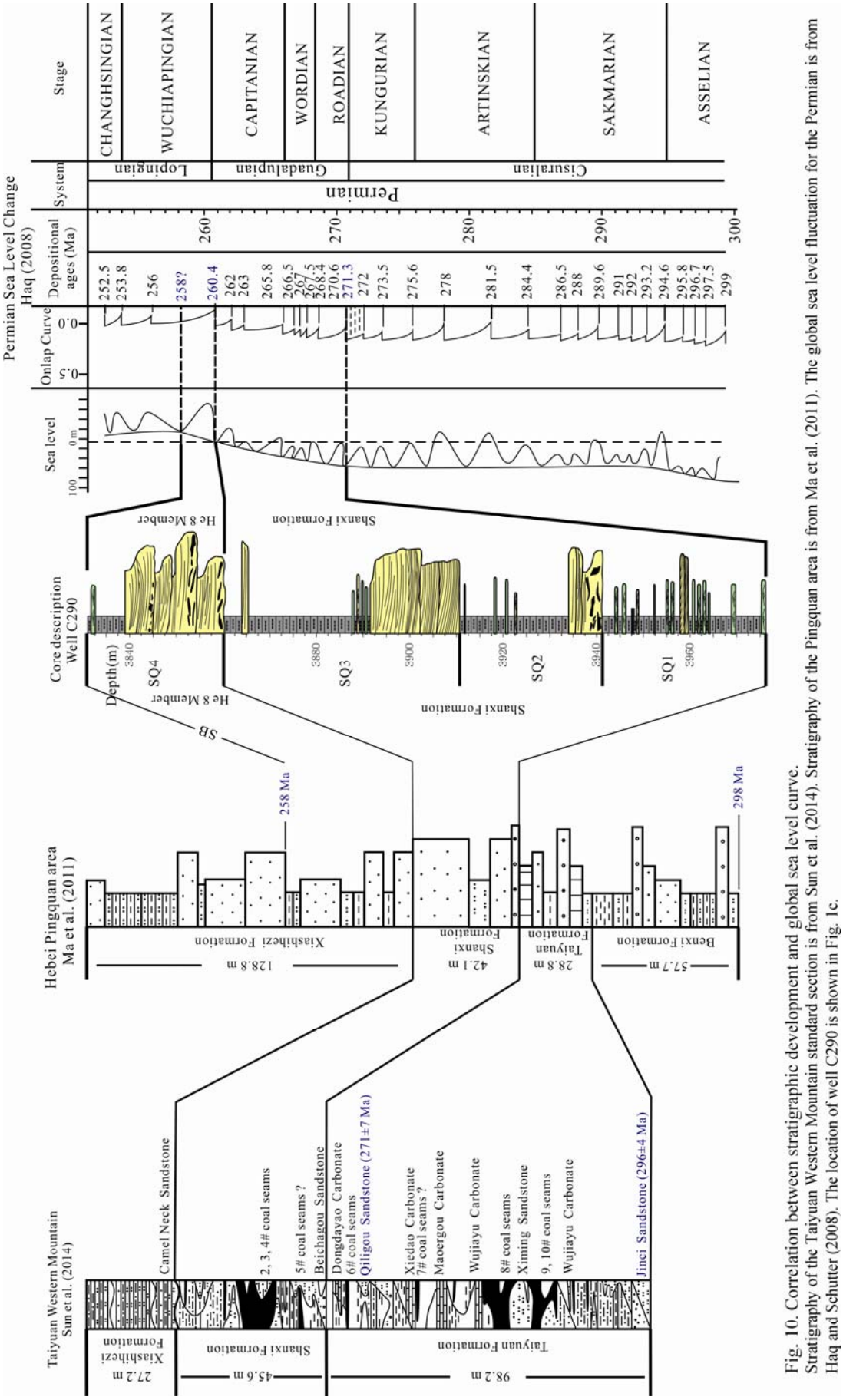

Fig. 10. Correlation between stratigraphic development and global sea level curve.
Stratigraphy of the Taiyuan Western Mountain standard section is from Sun et al. (2014). Stratigraphy of the Pingquan area is from Ma et al. (2011). The global sea level fluctuation for the Permian is from Haq and Schutter (2008). The location of well C290 is shown in Fig. 1c.

The whole sequence of the Shan 2 Member shows an overall fining-upward trend in the northeastern Ordos Basin (Zhu et al., 2008). The fluvial facies in the northeastern Ordos Basin had changed into deltaic facies in the southeast of the basin. We can identify three sequences in the Shanxi Formation in the southeast Ordos Basin (Figs. 9–10). Although it is impractical to assign each sequence to a sea-level fluctuation event, coarsening-upward sequences of the Shanxi Formation indicate a general regression trend (Figs. 9–10). Furthermore, the coal-bearing, relative fine grained Shanxi Formation to non coal-bearing, relative coarse grained He 8 Member in the Xiashihezi Formation reveals the sea level drop and paleoclimate changing into dry and cold. The emphasis of Chen et al. (2011) was on distinguishing marine and non-marine settings in the Shanxi Formation by utilizing geochemical and sedimentological signatures such as Sr/Ba ratio and clay mineral analysis. The dataset of Chen et al. (2011) further indicates that the sedimentation of the formation is dominated by a marine–continental system including fluvial, deltaic and tidal flat facies. That general interpretation with marine-continental facies is considered reasonable. Our data further shows that the delta developed in the Shanxi Formation is a tidal-influenced meandering river delta. The general coarsening-upward sequence of the Shanxi Formation shows a shallowing trend, evidenced by Sequence 3 (Upper Shanxi Formation), which has an obvious increase in sediment supply (Fig. 10). The shallowing-upward trend could be related to an overall sea-level fall from 271.3 Ma–260.4 Ma and stable basin subsidence in this period.

The He 8 Member (Sequence 4) is dominated by braided river delta deposits evidenced by coarse grain size, large-scale cross bedding, and a lack of clear tide-influenced signatures. The low-medium compositional and textural maturity and the lack of well-developed dark black mudstone indicate a weak reducing environment close to the source area, with a high sedimentation rate. These features imply a large-scale and strong sea-level fall, which created much sediment supply. The sea-level fall can be related to a significant global sea-level drop at 260.4 Ma. The zircon U–Pb age of the top of the He 8 Member also favors this argument (Fig. 10).

7.3 Paleotectonic and paleoclimate of Shan 2 Member–He 8 Member

Here we discuss the role of the paleoclimatic and paleotectonic conditions in controlling depositional sequence development and the relationships between sediment supply and accommodation space. Episodic tectonic instability has been proposed for the stratigraphic development of the He 8 Member in the Ordos basin, as reflected in the petrographic composition difference between the Shanxi Formation and the He 8 Member.

A significant and widespread climate change took place at the beginning and in the end of Shanxi Formation, which can be related to the Roadian, Wordian and Capitanian stages (Cope et al., 2005; Roscher and Schneider, 2006), and is recorded by a change from a humid-climate coal-bearing sequence (Shanxi Formation) to the Upper Permian arid-climate red beds. Increased chemical weathering and sediment influx of Sequence 1 in the Shanxi Formation can explain the high $^{87}Sr/^{86}Sr$ ratios. The meandering (Shanxi Formation) to braided (He 8 Member) deltaic evolution indicates an abrupt increase in sediment supply and transportation energy at the end of Shanxi Formation, which could be related to a significant sea-level fall or onset of uplift on the northern margin of the North China Block. The lowest $^{87}Sr/^{86}Sr$ ratio indicates a relatively dryer and colder climate compared with the Shanxi Formation. An explanation encompassing combined effect of sea-level drop and an uplift of the whole basin including the northern margin at the end of the Shanxi Formation seems reasonable. At the time of deposition of the Shanxi Formation, during 271 Ma–260.4 Ma, a general global sea level fall is already known (Fig. 10). The sandstone compositional difference between the Shanxi Formation and the He 8 Member, and an increase of sediment supply in the He 8 Member can be explained by a tectonic uplift.

7.4 Is the He 8 Member deposited in a marine or lacustrine setting?

The Shanxi Formation to the He 8 Member fit well to the global sea-level curve that shows an overall shallowing trend during 271 Ma–260.4 Ma (Fig. 10). A tectonic uplift at the end of the Capitanian Stage (Shanxi Formation) is suggested in this study. Based on facies analysis, tidal markers such as tidal rhythmites and mud drapes that are identified in the Shanxi Formation, a marine environment is indicated. In the mudstone of the Shanxi Formation and He 8 Member, a distinct $\delta^{13}C$ negative shift value of ~0.1‰ is observed and is too small to be considered as a sea-level change marker.

A lacustrine deltaic facies for the He 8 Member is favored by many groups (Chen et al., 2011; Tian et al., 2011), with which our facies analysis concurs (see Section 4.2). With the lack of tidal-influenced signatures, this lacustrine delta facies of the He 8 Member may have been influenced by the Paleo-Asian Sea for the following reasons: 1) Sequence 3 is thickest compared with the other three (Fig 9), which indicates that the base level fall is not very dramatic and the uplift is not significant; 2) a $\delta^{13}C$ negative shift of ~0.1‰ is not much compared with other

studies (Coniglio et al., 2000; Gomez et al., 2007; Van Geldern et al., 2006); and 3) the Ordos Basin (craton) is stable, and only a small uplift of the basin is recommended. To summarize, although a relative sea-level fall due to an uplift and eustatic sea-level drop is supported, the sedimentary system may still have been influenced by the Paleo-Asian Ocean.

8 Conclusions

Sedimentological analysis of the Shan 2 Member, Shan 1 Member and He 8 Member records 19 lithofacies, which group into two facies associations including tide-influenced meandering river delta and braided river to braided river delta. The sequence stratigraphy of the succession (Shan 2 Member to He 8 Member) allows us to determine four 3rd order depositional sequences separated by five sequence boundaries. Carbon, oxygen and $^{87}Sr/^{86}Sr$ analysis were also conducted to favor paleoenvironmental interpretation. A marine to marine-influenced lacustrine deltaic evolution in the Ordos Basin is suggested based on sedimentologic, sequence stratigraphic and stable isotopic studies. The depositional age of Shan 2 Member to He 8 Member spans ~13 Ma. A climate change from humid to arid is suggested through He 8 Member to Shan 2 Member. The He 8 Member in the Ordos Basin may still be influenced by paleo Asian Sea.

Acknowledgements

This paper was supported by National Natural Science Foundation of China (Grant No. 41472091), the Basic Scientific Fund for National Public Research Institute of China (Grant No. 2017Q08) and China Postdoctoral Science Foundation (Grant No. 2016M602087). The authors thankYanan Miao and Jiao Wang for their assistance in the field. Three anonymous reviewers and the editor Dr.Lian Liu and Dr. Susan Turner are thanked for their constructive comments and suggestions.

Manuscript received Mar. 1, 2017
accepted May 14, 2017
edited by Susan TURNER and Fei Hongcai

References

Allen, P.A., and Allen, J.R., 2013. *Basin Analysis: Principles and Application to Petroleum Play Assessment*. West Sussex: Wiley–Blackwell, 619 .

Beglinger, S.E., Doust, H., and Cloetingh, S., 2012. Relating petroleum system and play development to basin evolution: West African South Atlantic basins. *Marine and Petroleum Geology*, 30(1): 1–25.

Catuneanu, O., 2006. *Principles of Sequence Stratigraphy*. Armsterdam: Elsevier, 375.

Catuneanu, O., Galloway, W.E., Kendall C., Miall, A.D., Posamentier, H.W., Strasser, A., and Tucker, M.E., 2011. Sequence stratigraphy: methodology and nomenclature. *Newsletters on Stratigraphy*, 44(3): 173–245.

Chao, Y., 1925. On the age of the Taiyuan Series of North China. *Bulletin of the Geological Society of China*, 4(3–4): 221–250.

Chen, H., Li, J., Zhang, C., Cheng, L., and Cheng, L., 2011. Discussion of sedimentary environment and its geological enlightenment of Shanxi Formation in Ordos Basin. *Acta Petrologica Sinica*, 27(8): 2213–2229 (in Chinese with English abstract).

Coniglio, M., Myrow, P., and White, T., 2000. Stable carbon and oxygen isotope evidence of Cretaceous sea-level fluctuations recorded in septarian concretions from Pueblo, Colorado, USA. *Journal of Sedimentary Research*, 70(3): 700–714.

Cope, T., Ritts, B.D., Darby, B.J., Fildani, A., and Graham, S., 2005. Late Paleozoic sedimentation on the northern margin of the North China block: implications for regional tectonics and climate change. *International Geology Review*, 47(3): 270–296.

Dapples, E.C., 1947. Sandstone types and their associated depositional environments. *Journal of Sedimentary Research*, 17(3): 91–100.

Dickinson, W.R., and Gehrels, G.E., 2009a. Use of U–Pb ages of detrital zircons to infer maximum depositional ages of strata: A test against a Colorado Plateau Mesozoic database. *Earth and Planetary Science Letters*, 288(1–2): 115–125.

Dickinson, W.R., and Gehrels, G.E., 2009b. U-Pb ages of detrital zircons in Jurassic eolian and associated sandstones of the Colorado Plateau: Evidence for transcontinental dispersal and intraregional recycling of sediment. *Geological Society of America Bulletin*, 121(3–4): 408–433.

Flint, S., Aitken, J., and Hampson, G., 1995. Application of sequence stratigraphy to coal-bearing coastal plain successions: implications for the UK Coal Measures. In: Whateley, M.K.G., and Spears, D.A. (eds.), *European Coal Geology*. Geological Society, London, Special Publications, 82: 1–16.

Gomez, F.J., Ogle, N., Astini, R.A., and Kalin, R.M., 2007. Paleoenvironmental and carbon-oxygen isotope record of Middle Cambrian carbonates (La Laja Formation) in the Argentine Precordillera. *Journal of Sedimentary Research*, 77 (10): 826–842.

Haq, B.U., and Schutter, S.R., 2008. A chronology of Paleozoic sea-level changes. *Science*, 322(5898): 64–68.

Hu, C.Y., Qian, K., Wang, X.Q., Shi, Z.S., Zhang, G.W., and Xu, H.Z., 2010. Critical factors for the formation of an Upper Paleozoic giant gas field with multiple gas reservoirs in Ordos Basin and the transmutation of gas reservoir properties. *Acta Petrolei Sinica*, 31(6): 879–884 (in Chinese with English abstract).

Hu, J.M., Liu, X.S., Li, Z.H., Zhao, Y., Zhang, S.H., Liu, X.C., Qu, H.J., and Chen, H., 2013. SHRIMP U-Pb zircon dating of the Ordos Basin basement and its tectonic significance. *Chinese Science Bulletin*, 58(1): 118–127.

Izart, A., Stephenson, R., Vai, G.B., Vachard, D., Nindre, Y.L., Vaslet, D., Fauvel, P.-J., Suss, P., Kossovaya, O., Chen, Z.Q., Maslo,A., and Stovba, S., 2003. Sequence stratigraphy

and correlation of late Carboniferous and Permian in the CIS, Europe, Tethyan area, North Africa, Arabia, China, Gondwanaland and the USA. *Palaeogeography, Palaeoclimatology, Palaeoecology*, 196(1): 59–84.

Jones, J.V., Connelly, J.N., Karlstrom, K.E., Williams, M.L., and Doe, M.F., 2009. Age, provenance, and tectonic setting of Paleoproterozoic quartzite successions in the southwestern United States. *Geological Society of America Bulletin*, 121(1–2): 247–264.

Li, D., Shields-Zhou, G.A., Ling, H.F., and Thirlwall, M., 2011. Dissolution methods for strontium isotope stratigraphy: guidelines for the use of bulk carbonate and phosphorite rocks. *Chemical Geology*, 290: 133–144.

Li, J., Zhang, W., Luo, X., and Hu, G., 2008. Paleokarst reservoirs and gas accumulation in the Jingbian field, Ordos Basin. *Marine and Petroleum Geology*, 25(4): 401–415.

Li, S., Li, S., Shan, X., Gong, C., and Yu, X., 2017a. Classification, formation, and transport mechanisms of mud clasts. *International Geology Review*, 59: 1609–1620.

Li, S., Zhao, S., Liu, X., Cao, H., Yu, S., Li, X., Somerville, I., Yu, S., and Suo, Y., 2017b. Closure of the Proto-Tethys Ocean and Early Paleozoic amalgamation of microcontinental blocks in East Asia. *Earth-Science Reviews*, https://doi.org/10.1016/j.earscirev.2017.01.011

Li, Z., Wang, M., Yu, J., Han, M., Li, J., and Lv, D., 2006. Sequence stratigraphy of Late Paleozoic coal-bearing measures and the transgressive coal-formed features in Ordos Basin. *Acta Sedimentologica Sinica*, 24(6): 834–840 (in Chinese with English abstract).

Liu, J., Tian, J., Zhang, X., Zhang, S., Nie, Y., Zhao, Q., and Wei, D., 2006a. Depositional markers of marine transition facies and its evolution of Member 1 of Shanxi Formation, Tabamiao Area, North Ordos Basin. *Acta Sedimentologica Sinica*, 24(1): 36–42 (in Chinese with English abstract)

Liu, M., Mooney, W.D., Li, S., Okaya, N., and Detweiler, S., 2006b. Crustal structure of the northeastern margin of the Tibetan plateau from the Songpan-Ganzi terrane to the Ordos basin. *Tectonophysics*, 420(1): 253–266.

Ma, S., Meng, Q., and Qu, Y., 2011. A study of detrital zircons of Late Carboniferous-Middle Triassic strata in the northern margin of North China block and its geological implication. *Geological Bulletin of China*, 30(10): 1485–1500 (in Chinese with English abstract).

Mattauer, M., Matte, P., Malavieille, J., Tapponnier, P., Maluski, H., Xu Z., Lu, Y., and Tang, Y., 1985. Tectonics of the Qinling belt: build-up and evolution of eastern Asia. *Nature*, 317(6037): 496–500.

Miall, A.D., 1988. Architectural elements and bounding surfaces in fluvial deposits: anatomy of the Kayenta Formation (Lower Jurassic), southwest Colorado. *Sedimentary Geology*, 55(3): 233–262.

Nakazawa, T., Ueno, K., Nonomura, N., and Fujikawa, M., 2015. Microbial community from the Lower Permian (Artinskian–Kungurian) paleoclimatic transition, mid-Panthalassan Akiyoshi atoll, Japan. *Palaeogeography, Palaeoclimatology, Palaeoecology*, 420: 116–127.

Roscher, M., and Schneider, J.W., 2006. Permo-Carboniferous climate: Early Pennsylvanian to Late Permian climate development of central Europe in a regional and global context. In: Lucas, S.G., Cassinis, G., and Schneider, J.W. (eds), *Non-Marine Permian Biostratigraphy and Biochronology*. Geological Society, London, Special Publications, 265: 95–136.

Schumm, S., 1993. River response to baselevel change: implications for sequence stratigraphy. *The Journal of Geology*, 101(2): 279–294.

Sun, B., Zeng, F., Liu, C., Cui, X., and Wang, W., 2014. Constraints on U-Pb Dating of detrital zircon of the maximum depositional age for Upper Paleozoic coal-bearing strata in Xishan Taiyuan and its stratigraphic significance. *Acta Geologica Sinica*, 88(2): 185–197 (in Chinese with English abstract).

Tian, J.C., Wu, Q., Wang, F., Lin, X.B., Zhang, J.Q., and Cao, T.S., 2011. Research on development factors and the deposition Model of large area reservoir sandstones of He 8 Member of Xiashihezi Formation of Permian in Ordos basin. *Acta Petrologica Sinica*, 27(8): 2403-2412 (in Chinese with English abstract)

Vail, P.R.F., Audemard, S.A., Bowman, D., Eisner, N., and Perezcruz, C.,1988. The stratigraphic signatures of tectonics, eustacy and sedimentology-an overview. In: Einsele, G., Ricken, W., and Seilasher, A. (eds.), *Cycles and Events in Stratigraphy*. Springer-Verlag, Berlin, 617–659.

Van Geldern, R., Joachimski, M., Day, J., Jansen, U., Alvarez, F., Yolkin, E., and Ma, X., 2006. Carbon, oxygen and strontium isotope records of Devonian brachiopod shell calcite. *Palaeogeography, Palaeoclimatology, Palaeoecology*, 240(1): 47–67.

Wang, H., Shao, L.Y., Hao, L.M., Zhang, P.F., Glasspoo, I.J., Wheeley, J.R., Wignall, P.B., Yi, T.S., Zhang, M.Q., and Hilton, J., 2011. Sedimentology and sequence stratigraphy of the Lopingian (Late Permian) coal measures in southwestern China. *International Journal of Coal Geology*, 85(1): 168–183.

Wang, J., 2010. Late Paleozoic macrofloral assemblages from Weibei Coalfield, with reference to vegetational change through the Late Paleozoic Ice-age in the North China Block. *International Journal of Coal Geology*, 83(2): 292–317.

Wang, X., 2014. Major breakthrough of gas exploration in Yangchang blocks and its significance. *Oil and Gas Geology*, 35(1): 1–9 (in Chinese with English abstract).

Wang, W., Zhou, C., Guan, C., Yuan, X., Chen, Z., Wan, B., Wang, W., Zhou, C., and Guan, C., 2014. An integrated carbon, oxygen, and strontium isotopic studies of the Lantian Formation in South China with implications for the Shuram anomaly. *Chemical Geology*, 373: 10–26.

Xiao, X., Zhao, B., Thu, Z., Song, Z., and Wilkins, R., 2005. Upper Paleozoic petroleum system, Ordos Basin, China. *Marine and Petroleum Geology*, 22(8): 945–963.

Yang, Y., Li, W., and Ma, L., 2005a. Tectonic and stratigraphic controls of hydrocarbon systems in the Ordos basin: A multicycle cratonic basin in central China. *AAPG Bulletin*, 89 (2): 255–269.

Yang, R., Fan, A., Han, Z., and Tian, Y., 2005b. Geological features of natural gas pool formation in the Upper Paleozoic erathem in the Ordos Basin. *Journal of Shandong University of Science and Technology* (Natural Science), 24(1): 53–56 (in Chinese with English abstract).

Yin, A., and Harrison, T.M., 1996. *The Tectonic Evolution of Asia.* London: Cambridge University Press, 219.

Yuan, P., 1925. Carboniferous stratigraphy of northwestern Kansu. *Bulletin of the Geological Society of China*, 4(1): 29–

37.

Zhang, Z., Sun, K., and Yin, J., 1997. Sedimentology and sequence stratigraphy of the Shanxi Formation (Lower Permian) in the northwestern Ordos Basin, China: an alternative sequence model for fluvial strata. *Sedimentary Geology*, 112(1): 123–136.

Zhou, J., Wang, N., Zhao, Q., Lin, G., Yin, X., and Gao, F., 2014. Petrology characteristics of the Upper Paleozoic sand reservoir in the southeast Ordos Basin. *Bulletin of Mineralogy, Petrology and Geochemistry*, (4): 500–504 (in Chinese with English abstract).

Zhu, H., Chen, K., Liu, K., and He, S., 2008. A sequence stratigraphic model for reservoir sand-body distribution in the Lower Permian Shanxi formation in the Ordos Basin, northern China. *Marine and Petroleum Geology*, 25(8): 731–743.

About the first author

SHAN Xin: Male; born in 1988 in Mishan City, Heilongjiang Province; PhD; postdoc of First Institute of Oceanography, SOA; he is interested in sedimentary geology. Email: xshan@fio.org.cn; phone: 18561322933.